Plasma Sources Science and Technology

ACCEPTED MANUSCRIPT

Light scattering by subwavelength Cu_2O particles

To cite this article before publication: Kaleem Ullah *et al.* 2017 *Nanotechnology* **28** 134002.
https://doi.org/10.1088/1361-6528/aa5e3c

Light Scattering by Subwavelength Cu_2O Particle

Kaleem Ullah[1], Xuefeng Liu[1,*], N.P.Yadav[1], Muhammad Habib[2], Li Song[2] and Braulio García-Cámara[3]

[1] School of Electronics Engineering and Opto-electronic Technology, Nanjing University of Science and Technology, Nanjing, 210094, P.R. China
[2] National Synchroton Laboratory, University of Science and Technology of China, Hefei, P.R. China.
[3]Group of Displays and Photonic Applications (GDAF-UC3M). Carlos III University of Madrid. Leganes, 28911 Madrid, Spain.

E-mail: liuxf1956@163.com

Abstract

Novel metamaterials with new capabilities to manipulate light may be performed by considering basic building blocks with new optical properties. This is the case of resonant magneto-dielectric particles. In this work, the resonant response of high-dielectric Cu_2O subwavelength particle is analyzed, both analytically and experimentally. The emergence of electric and magnetic resonances and their interferential effects, producing directional behaviors, can be used in a new generation of metamaterials, as well as new integrated optical devices.

Keywords: Metamaterial, Subwavelength, Resonances, Scattering, Directionality.

1. Introduction

Controlling the visible light with subwavelength particles has been subject of great interest in many applications; for instance, improving the efficiency of the solar cell [1], increasing the sensitivity of the optical sensors [2,3], realizing optical nano-circuits [4], and generating engineered materials, or metamaterials [5], with non-natural optical properties. These novel materials present effective properties as consequence of the optical properties of their basic building blocks, but also due to their size, shape, density and geometrical configuration. By manipulating these parameters, the effective properties can be tuned à la carte [6]. In this sense, the effective optical properties of metamaterials may be far beyond those of natural materials, allowing even negative refraction [7]. To achieve the required subwavelength control of light, basic building blocks are usually plasmonic nanoparticles made of noble metals (e.g. gold, silver). These are applied for these purposes due to their ability to support localized surface plasmons (LSPs) [8,9]. However, substantial energy losses are inevitable in these particles, especially at visible light wavelengths, because of the presence of free electrons and their Ohmic losses. This drawback has hampered the realization of the aforementioned applications using metallic plasmonic nanoparticles [10]. Recently a new branch of nano-photonics has emerged through the manipulation of strong optically-induced Mie-type electric and magnetic resonances in dielectric and semiconductor nanoparticles with high refractive index [11, 12]. High-index resonant nanoparticles offer many advantages over their plasmonic counterparts in terms of reduced dissipative losses, low heating, and the resonant enhancement of both electric and magnetic fields [13]. These resonances are a consequence of the spatial distribution of light inside the particles, allowing configurations compatible with both electric and magnetic resonances. This magnetic response in non-magnetic materials may be one of the most important advantages of the use of high-index dielectric particles in the design of future metamaterials. While an artificial magnetism in the visible range has been achieved until now by using arrangements of nano-resonators (i.e. split-ring resonators) [14] or by means of particles with complex geometries [15], dielectric particles with simple geometries (e.g. spheres, cylinders, cubes) may be used as building blocks presenting a magnetic response themselves. In addition, the interaction between the different electric and magnetic multipolar modes supported by these particles is an important step forward the total control of light at the nanoscale. The coexistence of electric and magnetic resonances has enabled the experimental realization of Kerker's conditions [16] for reflectionless scattering by using individual dielectric nanoparticles [17,18], a development that subsequently allows various new phenomena for manipulation of directional light scattering [19-21] and optical nano-antenna applications [22–24].

While the fabrication of silicon nanoparticles is not trivial, researchers are currently analyzing other materials supporting these Mie resonances. Germanium (Ge), gallium arsenide (GaAs) are common materials in integrated photonics with this kind of response [25, 26]. In this work, we introduce a new alternative material. In particular, we analyze the scattering properties of subwavelength particles made of a copper (I) oxide (Cu_2O), whose optical properties are adequate to support Mie scattering resonances. This material has already potential applications in fields like solar energy conversion, catalysis and gas sensors, that maybe improved by the emergence of these resonances, enlarging its applicability. Both theoretical and experimental techniques have been used in this work. In this sense, we have investigated the near field scattering properties of a subwavelength particle using a scattering type scanning near-field optical microscopy s-SNOM. Apertureless or scattering type s-SNOM [27] has managed to map both the local amplitude and phase of the Mie modes by interferometric detection of the antenna fields scattered by a scanning atomic force microscope tip [28–31]. Along with the near field scattering of the Cu_2O particle, we also described here its polarization status by using a high-resolution polarimetric technique named as polarization Parametric Indirect Microscopic Imaging (PIMI). This technique may offers a new way to obtain information from resonant nanoparticles. PIMI is a far field super resolution microscopy, modulates the field variation details to the atomic arrangement of the matter inside the particle

composite structure and outer shape of the particle. It is then resolve the above characteristics of the sample under test (SUT) by filtering the measurement noise due to diffraction in the light path to reach sub-wavelength super-resolution, breaking the diffraction limit, and has the potential to pick up and resolve more near field scattering characteristics reaching even higher resolving power [32, 33]. The experimental results have been checked using theoretical methods based on Mie theory and numerical techniques to solve Maxwell's equation in and around the scatterer.

2. Methods

2.1 Theoretical background

The scattering response of small particles in the far- field region is well described by the Lorentz-Mie theory [34]. This method proposes a solution of Maxwell's equation by considering the electromagnetic fields as an infinite expansion of vectors spherical harmonics. According to this, the interaction between light and a particle may be quantified using the scattering (Q_{sca}), absorption (Q_{abs}) and extinction (Q_{ext}) efficiencies, which are analytical expression given as:

$$\begin{aligned} Q_{sca} &= \frac{2}{x^2}\sum_{n=1}^{\infty}(2n+1)\left(\left|a_n\right|^2+\left|b_n\right|^2\right), \\ Q_{ext} &= \frac{2}{x^2}\sum_{n=1}^{\infty}(2n+1)\,\mathrm{Re}\left(a_n+b_n\right), \\ Q_{abs} &= Q_{ext}-Q_{sca}, \end{aligned} \tag{1}$$

Where x, the size parameter, is defined as the product of the incident wavenumber and the particle radius ($x=k\cdot R$). a_n and b_n are the scattering Mie coefficients which quantify the weight of the electric and magnetic contributions, respectively, in the scattering response. In addition, their order (n) is directly related with the multipolar character of the response. In this sense, $n=1$ corresponds to a dipolar response, $n=2$ to a quadrupolar one and so on.

Considering subwavelength nanoparticles, these infinite series are truncated to a finite one which limit order depends on the radius/wavelength ratio [35]. This multipolar description allows to identify the dominant character in light scattering or the nature of the emergent resonant modes. The optical properties of Cu_2O were obtained from Sopra database [36].

Lorenz-Mie theory also describes the spatial distribution of light scattering around the particle in the far-field region. In this sense, the two orthogonal components of the polarized scattered irradiandance (normalized to the incident intensity) are expressed as follows [34].

$$\begin{aligned} I_{\parallel} &= \left|\sum_n \frac{2n+1}{n(n+1)}\left(a_n\cdot\tau_n+b_n\cdot\pi_n\right)\right|^2, \\ I_{\perp} &= \left|\sum_n \frac{2n+1}{n(n+1)}\left(a_n\cdot\pi_n+b_n\cdot\tau_n\right)\right|^2, \end{aligned} \tag{2}$$

In Eq, (2), the functions π_n and τ_n are the responsible of the angular dependence. They introduce it through the scattering angle θ *and* are defined as follows [34].

$$\begin{aligned} \pi_n &= \frac{P_n^1}{\sin\theta}, \\ \tau_n &= \frac{dP_n^1}{d\theta}, \end{aligned} \tag{3}$$

Where P_n^1 is the *associated Legendre function* of first kind of degree n and order 1. While polarized components are very important in non-spherical particles, in this case, there is no polarization sensitive due to the spherical symmetry of the experimental samples.

The co-existence of several multipolar, electric or magnetic, contributions in the same scatter may induce the appearance of interferential phenomena between them. These interferences are the responsible of interesting optical phenomena like Fano resonances [37–39] and scattering directionality [40]. In this later case, light scattering may be cancelled or drastically reduced either in the backward or the forward direction by the destructive interference of the electric and the magnetic dipolar contributions. Kerker and co-workers firstly described these effects in reference [16]. They established that scattering directionality is possible under certain relations between the Mie coefficients. In particular, a minimum forward scattering is achieved at those wavelengths where $a_1=-b_1$ while there

is no backward scattering at those wavelengths satisfying that $a_1=b_1$. These phenomena have been experimentally shown using high-permittivity dielectric nanoparticles, which can support both electric and magnetic resonances in the visible range [41, 42]. Scattering properties in regions far from the scatterer are quite interesting in several applications, however the near-field distribution of the electromagnetic field is a key point in the design of complex metamaterials or integrated photonic devices because it determines the optical interactions with neighbors. Unfortunately, near-field analysis requires larger efforts than in the far-field. For this reason, numerical simulations are usually performed to analyze it. In this work, we used Finite Difference Time Domain (FDTD) and Finite-Element Method (FEM) to study the near field as well as far field distribution of the scattered field. In our simulation using method FDTD, we used a Gaussian source and frequency domain field monitor. A converging test is performed by starting the simulation with a coarse mesh and reducing the mesh-cell size until consecutive simulations produced closely matched results. A converging test is performed initially for the silicon substrate, when there is no nanoparticle present, followed by a converging test for the nanoparticle. The final mesh cell for the silicon substrate is 10 nm x 10 nm x 1 nm and for the particle is equal to $R_p/15$, where Rp is the radius of particle. The simulation time was set to 1000fs, which is about 10 times larger than the time required by the simulation to converge. At the end of each simulation though, we also ensure that all field components have decayed to zero, which means that the simulation has run for sufficiently long time for the Fourier transformation to be valid.

In FEM simulation, we used same incident angle and other conditions reproducing the experimental ones in the s-SNOM experiment. We used a *x*-polarized plane wave and a fine tetrahedral mesh unlike in FDTD simulations and used the red-yellow color bar which provides us a good comparison between the experimental and simulation results. To absorb light scattered in all directions, the entire simulation region was surrounded by a perfectly matched layer (PML and scattering boundary conditions were imposed on PML boundaries to preclude reflections. We also performed the FEM simulation for calculating the Stokes for the comparison of the Stokes given by PIMI method [32,33].

2.2 Sample Preparation

Crystalline Cu_2O nanoparticles were synthesized by adopting a simple solution method. Reagents used in the synthesis procedure were of research grade (Sigma-Aldrich). For synthesis procedure first desired molar ratio of PVPMW 30000 (polyvinylpyrrolidone) and $CuCl_2.2H_2O$ (cupric chloride dehydrate, 0.01 mol·L^{-1}) was achieved by slowly added PVP into $CuCl_2.2H_2O$ solution drop by drop. $NaOH$ solution (2.0 mol·L^{-1} of an amount of 10 ml.) was mixed into transparent $PVP\text{-}CuCl_2.2H_2O$ solution. The solution was stirred for 30 minutes then 10 ml. ascorbic acid (0.6 M) was added to the above solution and then let it aged for 3 hours. Stirring and heating were performed in a water bath. Centrifugation and decanting were performed to get required precipitate. After washing with deionized water and ethanol precipitate was dried in an oven for several hours. The very detailed experimental conditions are reported in reference [43]. Experimental samples were analyzed by SEM (scanning electron microscopy) to determine their shape and size. Fig. 1(a) shows a SEM image of one of these samples. This shows a spherical particle with a radius around 130 nm. The typical synthesis process gives Cu_2O spherical particles of different sizes. To choose a particular particle with a certain size and well-defined spherical shape, we prepared a marked substrate. Marks on the substrate were made using successive procedure of coating and developing of photo resist with the help of photo lithography (MA/BA6 Mask and Bond Aligner, Süss Micro Tec). Then, with the help of scanning electron microscope (Gemini 500, ZEISS), the position of the specific sphere was marked with remarkable marks on the substrate so that later on we can study that particular sphere for other characterizations.

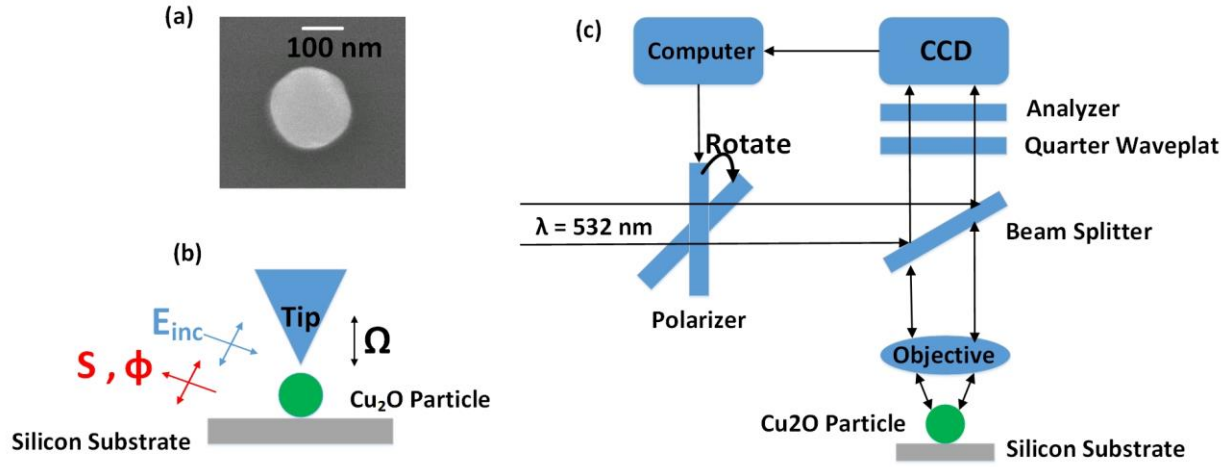

Figure 1. (a) SEM image of a Cu_2O nanoparticle. (b) Scheme of the near field imaging of s-SNOM. Tip scans the Cu_2O nanoparticle starting from coordinate (0,0,0). E_{inc} illuminates under a certain angle and backscattered light is detected as amplitude S and angle ϕ, (c) Scheme of the polarization PIMI for the measurement of the Stokes parameters.

2.3 Experimental Characterization with s-SNOM and PIMI Techniques

The s-SNOM (scattering-type Scanning Near-field Optical Microscope) used in our experiment is based on an atomic force microscope (AFM) with both disk and tip being illuminated from the side with P-polarized He-Ne laser light (see Figure 1(b)). The measurement consists in the detection of light scattered from the tip that scans the samples. The AFM is operated in tapping mode where the tip is vibrating mechanically in z-direction with frequency of 300 kHz and an amplitude of Ω=20 nm, thus demodulation of the scattered far field allows for suppression of background scattering and for recovering the near-field signal. Heterodyne interferometric detection yields amplitude S_n and phase ϕ signals with n being the nth harmonic of the tapping frequency. Along with the near field scattering of the Cu_2O particle, we also described its polarization status by using a high resolution polarimetric technique named as Parametric Indirect Microscopic Imaging (PIMI). The polarization parametric indirect microscopic image (PIMI) system, as shown in Fig. 1(c), consists of an Olympus reflection microscopic system BX51M that provides the basic optical path. We also incorporated a home-made system in the optical path. This is composed of a polarization modulation module with an angle precision of 0.05 degree and a Basler (PiA2400-17gm) CCD with a pixel resolution of 3.45 micron. The 3.45-micron-pixel CCD resolution leads to an outmost potential resolving power of 34.5nm if diffraction limit is broken and Nyquist principle is fulfilled in the microscopic system, working with a 100x objective. The direct and indirect optical images were carried out at illumination wavelength of 532nm (typical wavelength of the second harmonic of a Nd:YAG laser). PIMI is a far field super resolution microscopy, modulates the field variation details to the atomic arrangement of the matter inside the particle composite structure and outer shape of the particle. Then, it is resolve the above characteristics of the sample under test (SUT) by filtering the irrelevant scattering from neighboring source points in the SUT to reach sub-100 nm super-resolution, breaking the diffraction limit, and it has the potential to pick up and resolve more near field scattering characteristics reaching even higher resolving power [32,33].

3. Results and Discussion

3.1 Scattering Resonances

Copper (I) oxide or Cu_2O is a dielectric material with semiconducting properties and a real refractive index (n) around 3 in the visible range. This value allows that spherical particles made of Cu_2O may support light scattering resonances. In this sense, Figure 2 shows the extinction efficiency (Eq. 1) of a spherical particle of Cu_2O with a radius of 130nm, like that showed in Fig. 1(a), as a function of the incident wavelength. The spectral profile shows a clear resonant mode at large wavelengths, while a small resonant peak is also observed around 600nm. In order to identify the dominant multipolar contributions and also to determine the character of the resonance, Fig. 2 also shows the first four multipolar contributions of the extinction efficiency. These correspond to the electric and magnetic dipolar and quadrupolar contributions. From this, it is clear that Cu_2O particles have both electric and also magnetic character, as it was previously reported in other semiconductor nanoparticles [11]. In fact, the dominant resonance observed at 750nm corresponds to a dipolar magnetic resonance. On the other hand, electric dipolar effect reaches a maximum at 631nm, which corresponds with the small resonant peak observed in the extinction efficiency. Quadrupolar effects have not remarkable effects in the considered range. Higher orders than the quadrupolar ones have negligible contributions, for this reason, they are not included.

The origin of these effective multipolar contributions lies on the spatial distribution of light inside the particle, as it was commented

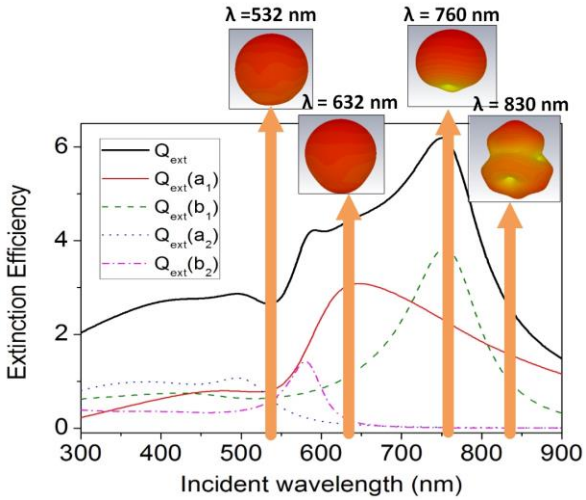

Figure 2. Extinction efficiency (solid line) of an isolated Cu_2O nanoparticle (R=130nm) as a function of the wavelength of the illumination beam. The contributions of the first four multipolar terms (a1, a2, b1 and b2) to the extinction efficiency have been also included to identify the character of the scattering at different wavelengths. The scattering patterns at different wavelengths have been also included.

above [35]. In addition, the near-field distribution is a key point in the design of complex metamaterials [44]. For this reason, numerical simulations have been performed to study this distribution at different remarkable incident wavelengths. Figures 3 and 4 show FDTD simulations of the scattered field around and inside the particle to observe the EM distribution considering two orthogonal planes. In Fig. 3, the near field distribution is showed in the plane containing the magnetic field (YZ plane), whereas in Fig. 4 these distributions belong in XZ plane, the one containing the incident electric field.

The complexity of the electromagnetic response of this particle is well observed at low wavelengths. In this range, the weight of the different multipolar contributions is equivalent (see Fig. 3(b)) making that the spatial distribution of the scattered electric field is not well-defined. The first considered wavelength, λ=532 nm, shows an example of this behavior. As can be seen in Fig. 3 (c), the electric-field distribution of light inside the particle has several maxima and minima, at least 3 are well observed, producing a complex profile out of the particle. This is also observed in Fig. 4(c). However, in this plane, the electric quadrupolar profile come out more clearly than other ones, with four lobes surrounding the particle.

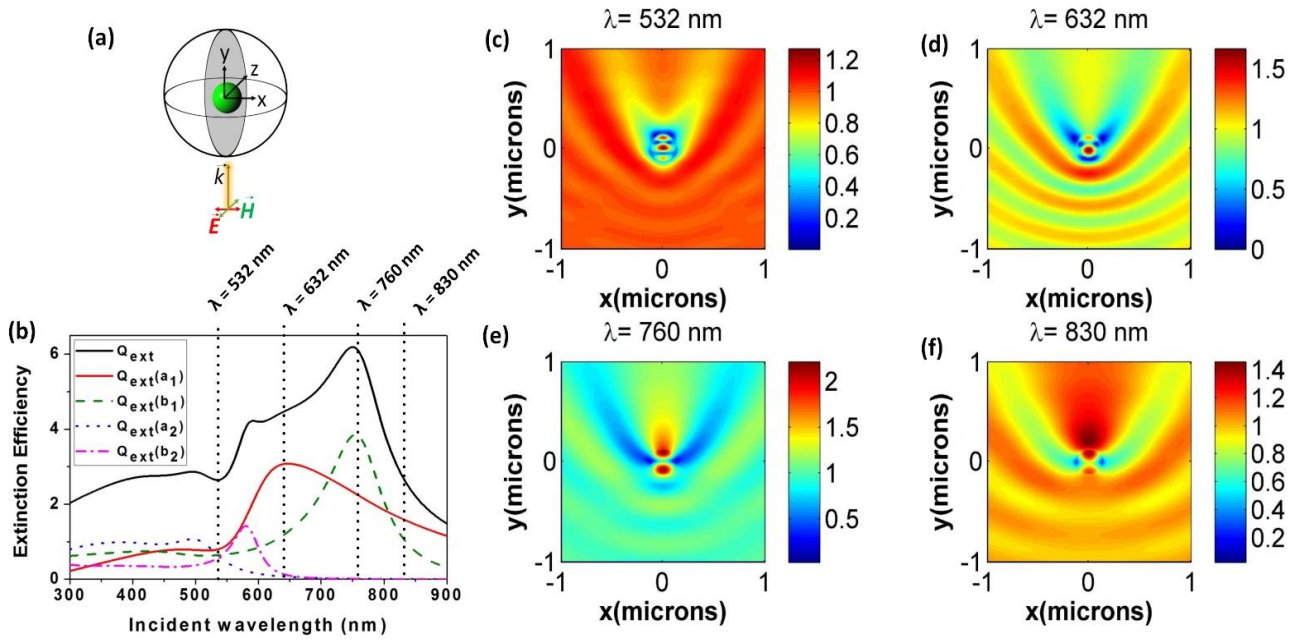

Figure 3. Simulated distribution of the scattering electric field around the considered particle at four remarkable wavelengths in YZ plane as shown from the geometry depicted by (a). Insets show the geometrical configuration and the extinction efficiency at the considered wavelengths as well as the dominant multipolar contributions.

Those wavelengths corresponding to the maximum values of the dipolar contributions are quite interesting due to its well-defined profile and its potential use in future applications, like novel metamaterials. Figures 3 and 4 (d) correspond to an incident wavelength of λ=632 nm. At this wavelength, the electric dipolar contribution achieves a maximum. Then, the scattering is expected to resemble that of an electric dipole. This is clearly observed out of the particle in Fig. 4(d). Light scattering in mainly focused in the sides of the particle, forming to well-defined lobes and in the same direction of the polarization of the incident electric field. In this case, lobes are slightly shifted to the forward direction probably to the effect of the silicon substrate. The information given by the distribution of scattered field in Fig. 3(d) is less clear, however, the strong concentration of the scattered field inside the particle is consequent with the excitation of an electric dipole, as expected. The scattering simulated response at λ=760 nm is shown in Figures 3 and 4 (e). At this wavelength, light scattering is maximum and corresponds to the excitation of a magnetic dipolar resonance. The origin of this magnetic effect lies on the

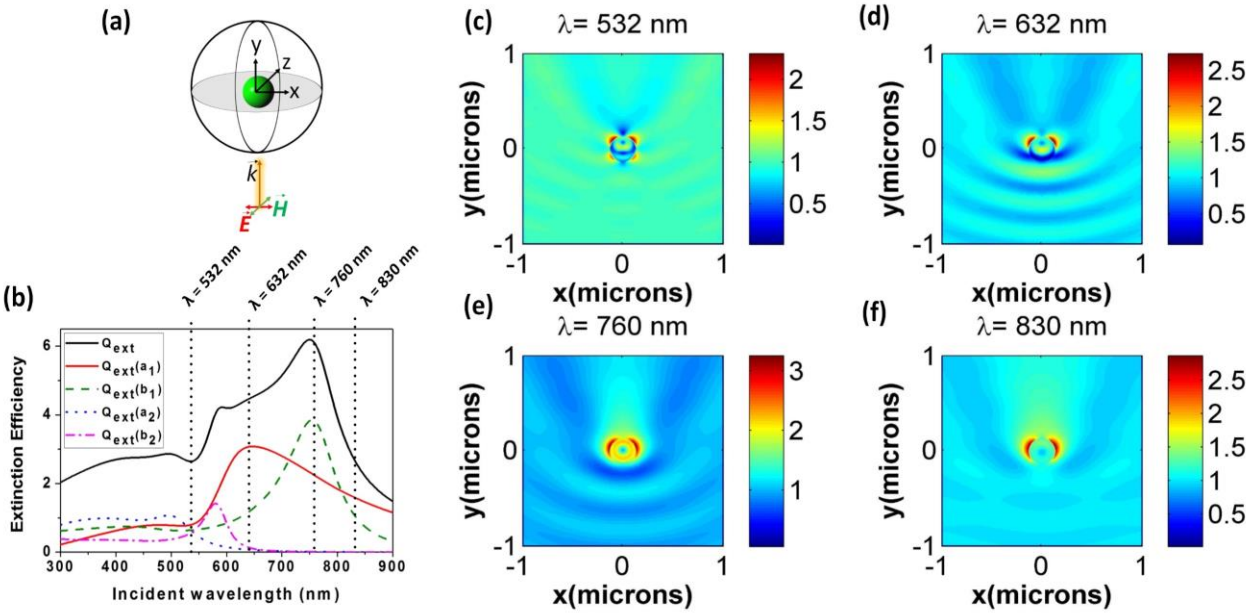

Figure 4. Simulated distribution of the scattering electric field around the considered particle at four remarkable wavelengths in a scattering plane normal to the incident direction. Insets show the geometrical configuration and the extinction efficiency at the considered wavelengths as well as the dominant multipolar contributions.

circulation of the electric field inside the particle, as it can be seen in Fig. 4(e), the circular distribution of the field inside the particle resembles an electric turn, producing an effective magnetic dipole [11]. This effect is also seen in the transversal plane (Fig 3 (e)), where the scattered electric field has the profile of a transversal view of a toroid. The last considered case is that related with a λ=830 nm at which only dipolar contributions have non-negligible effects. In fact, both multipolar contributions acquire similar weights. For this reason, there is no a dominant behavior. In this sense, while in the plane parallel to the electric field (Fig. 3(f)), the distribution of the scattered electric field is consistent with the excitation of the magnetic mode, in the orthogonal plane (Fig. 4(f)), the distribution is close to that of an electric mode.

3.2 Angular scattering distribution

Besides the scattering resonances, the angular distribution of the scattered light is very important, either in the far or the near field, and its control is basic in the design of current and future photonics devices. While the near-field distribution may govern the neighbor interactions and then in the effective properties of a metamaterial [43], the far-field distribution is capital in their use as nanoantennas. As mentioned above, the coexistence of electric and magnetic modes at the same incident wavelength in dielectric particles may produce interferential effects between them leading to unexpected phenomenal, like scattering directionality. Kerker and co-workers established in reference [16] certain conditions producing zero forward or zero-backward scattering in magneto-dielectric small particles. These conditions, known as Kerker's conditions, may be enunciated using Mie coefficients as $a_1=-b_1$ and $a_1=-b_1$, respectively and they have been experimentally shows in references [19, 20]. However, the presence of substrate usually makes difficult the observance of these effects, in particular, the zero-forward scattering. In this section, we have analyzed the near-field scattering patterns of the considered particles searching directional effects. Figure 2 shows the far-field distribution of light scattering at four different wavelengths. The yellow arrow represents the direction of the impinging light. These shown that there is a dominant forward scattering with a maximum directionality at the maximum of the extinction (λ=760nm). While Kerker's conditions of an isolated Cu_2O are located at 713 nm (zero-forward) and 808 nm (zero-backward), we guess that the presence of a substrate strongly changes their observance producing this directionality. It is also important to remark that light scattering is drastically reduced in the forward direction and focused to the backward one in 830nm, trying to resemble a minimum-forward scattering.
The angular scattering distribution in the near-field region was measured using s-SNOM techniques. Whereas in the working wavelength of the s-SNOM, i.e. 632 nm, the directionality is not as significant as in the case of 760 nm. For this reason, we consider different sizes of the particles, in such a way that certain directionality may be observed at the experimental wavelength. In particular, three different particles with radius of 110 nm, 120 nm and 145 nm were considered. The three particles sizes have a mean of 130 nm and these particles present a certain degree of directionality at the working wavelength. In those measurements, the incident angle was 55º with respect to the substrate.

By following the experimental setup of the s-SNOM, we have performed the FEM near field scattered simulation which has delivered a nice match between these results as shown in Fig. 5. In FEM simulation, the amplitude of the near scattered e-field has been achieved by adding the three orthogonally components. With the help of FEM simulations, we also calculated the phase, which also shows a similar pattern as of the experimental one. The scale bar shows in Figure 5 having a length equal to 500 nm. Some near field distribution has been destroyed in the experiment due to some noise caused by the scanning nano probe of the s-SNOM whose deficiency has been fulfilled by our FEM simulations as shown in Fig. 5(c, d). In this case, light scattering reaches a maximum in the forward direction but without a lack of light in the backward one, in consonance with the far-field distribution shown in Fig. 2. With the aim of searching a larger degree of directionality, we have measured the angular scattering distribution of two more nanospheres with particle radius of 110 nm and 140 nm. While the smallest particle does not have a clear directionality, the largest one presents a dominant scattering in the forward direction.

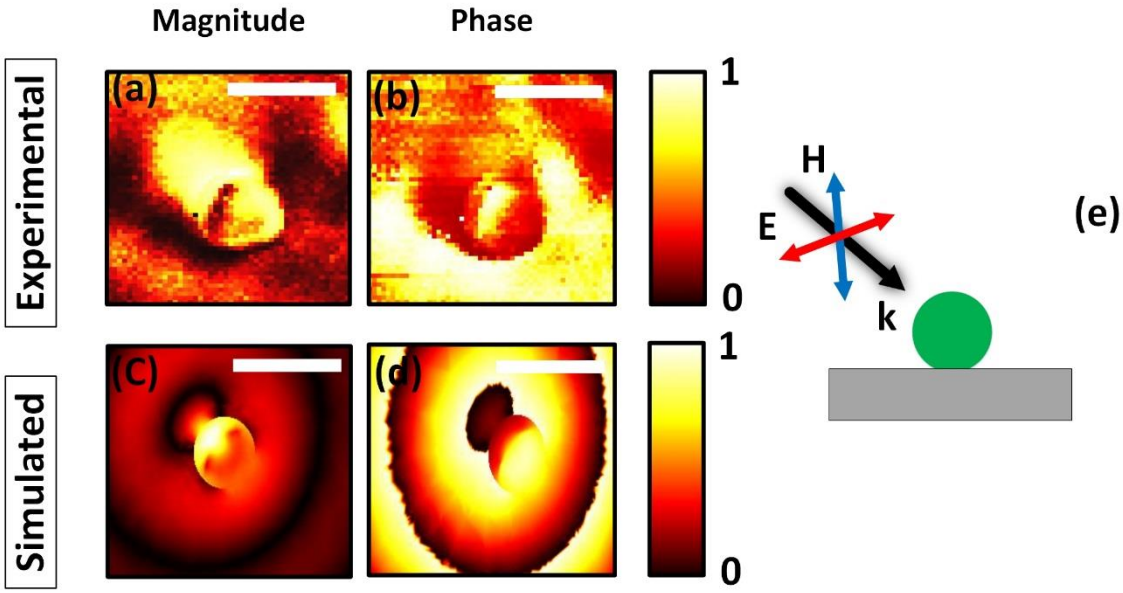

Figure 5. Measured near field scattering distribution using s-SNOM, both magnitude (a) and phase (b). Simulated near field scattered field, magnitude and phase are plotted (c) and (d) respectively, using FEM methods. A scheme of the geometrical conditions and the incident light is shown in (e).

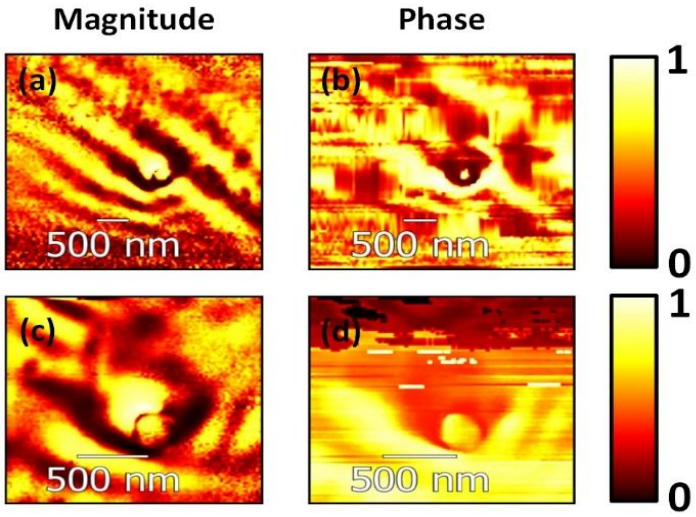

Figure 6. Measured near field scattering distribution using s-SNOM of a Cu_2O particle with a radius of 110 nm, both magnitude (a) and phase (b) are included. The magnitude (c) and phase (d) of a particle with a radius of 140 nm was also measured using s-SNOM.

Along with measuring the direct near-field scattering, we also measured the indirect scattering distribution via Stokes parameters which showing the information about the polarization status together with the scattering field distribution of the 130nm radius Cu_2O particle using our super resolution polarimetric technique PIMI (Parametric Indirect Microscopic Imaging). PIMI system was built by modifying the conventional far field microscopy in such a way that the variation of the polarization status of impinging light can be precisely controlled, imaging was subsequently acquired by analyzing the dependence of the optical intensity transmitted through or reflected from the samples on the incident light polarization status. When this modulated polarized light meets with the sample with strong anisotropy, the near to far field coupling effects produces well known changes of the optical field at each image point in the far field. By

tracking and measuring these changes at each pixel of the image, we can fit the curve and the point spread function (PSF) become narrower, resulting in breaking the diffraction limit. In this way, we can get the information about the scattered near field signals which contains the subwavelength information in the far field region. Stokes parameters have been calculated by using a birefringence model because the birefringence effect occurs in the sample during the light wave propagation [33]. In Fig. 7, our indirect parameters give us information of the azimuthal spatial scattering variation about the spatial distribution of the scattered field which cannot be detected with conventional microscopy [33]. Our FEM simulation proved the Stokes scattering distribution, including the imaging information which has been lost in the PIMI imaging. This mapping of the spatial scattering distribution around a subwavelength particle with the use of the far field microscopy is not usual, which is due to the filter off the irrelevant diffraction from the neighboring source points and fitting the curve at each pixel of the image. In this way, we can retrieve a lot of information which has been lost in the conventional far field microscopy due to the diffraction limit. As can be seen in the Fig. 7, in the S_0 and S_1 image, the inner lobe information has been lost in both the experimental as well as the simulated results, whereas in the imaging of the S_2 and S_3, the simulated results have explained the inner lobe information, however it has been lost in experimental imaging of S_2 and S_3 like S_0 and S_1 due to the less birefringence effect produced on the center surface of the Cu_2O particle.

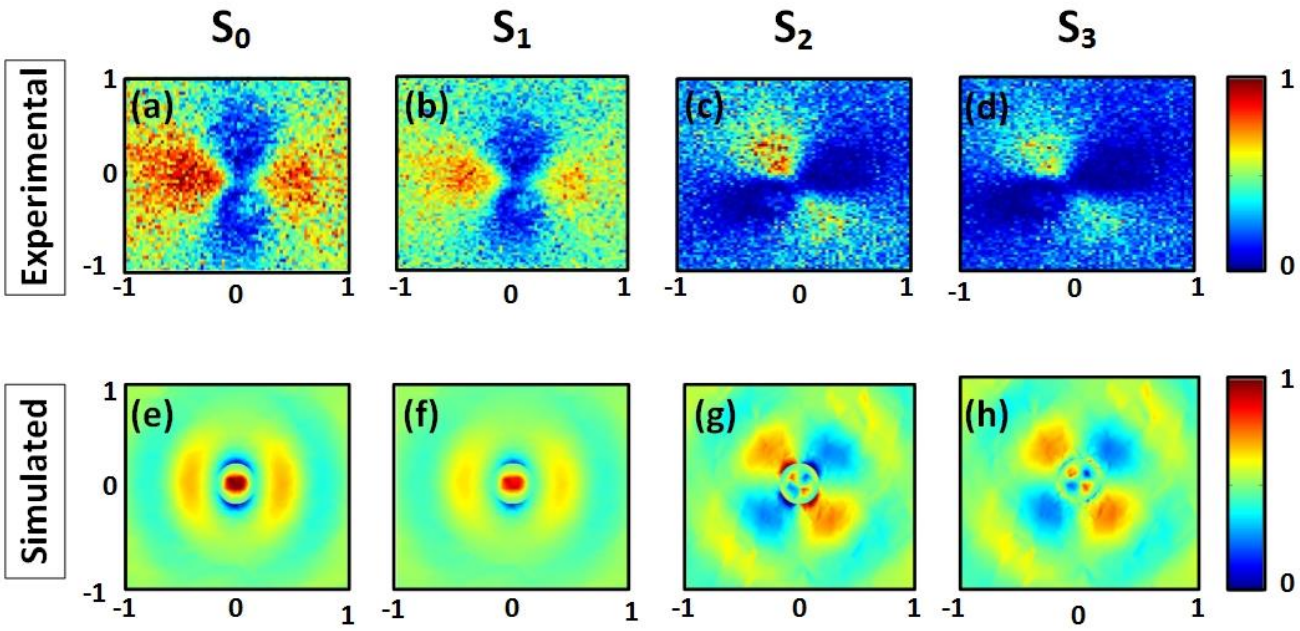

Figure 7. Stokes parameters of a Cu_2O particle with a radius of 130 nm obtained using PIMI technique (upper panel) and numerical techniques (lower panel) at wavelength 532nm.

4. Conclusions

In a summary, we have analyzed the scattering properties of Cu_2O nanoparticles from a theoretical and experimental point of view. We showed that these particles are able to support electric and magnetic resonances in the visible range of electromagnetic field. The numerical calculation of the scattered field, both in the inner and the external part of the particle, shows the origin of these multipolar contributions. In addition, the angular scattering distributions have been analyzed to find directional scattering. While far-field distributions have been numerically calculated, the near-field distribution is shown using s-SNOM. The restricted incident wavelength of s-SNOM requires the use of different particle sizes in order to observe directional scattering. Using that, dominant forward scattering can be observed. In addition, numerical calculations with FDTD and FEM methods have been carried out to prove the experimental results. These results show that Cu_2O particles are potential building blocks of future metamaterials with abilities to manipulate magnetic field or to control light scattering directionality. These properties are quite interesting in a large range of applications, from optical nanodevices to the electromagnetic cloaking.

Acknowledgements

The authors wish to acknowledge the financial support by National Science Foundation China (NSFC) No. 61275163, 61501239, 61605078, 61604073 and the "Zijin Professor Project" of Nanjing University of Science and Technology. BGC also wants to acknowledge the support by Ministerio de Economia y Competitividad of Spain (TEC2013-47342-C2-2-R) the RD Program of the Comunidad de Madrid (SINFOTON S2013/MIT-2790) and COST Action IC1208.

References

[1] Atwater H A and Polman A 2010 Plasmonics for improved photovoltaic devices *Nat. Mater.* **9** 865–865

[2] Nie, S. and Emory S-R 1997 Probing Single Molecules and Single Nanoparticles by Surface-Enhanced Raman Scattering *Science (80-.).* **275** 1102–6

[3] Shibanuma T, Albella P and Maier S A 2016 Unidirectional light scattering with high efficiency at optical frequencies based on low-loss dielectric nanoantennas *Nanoscale* **8** 14184–92

[4] Engheta N 2007 Circuits with light at nanoscales: optical nanocircuits inspired by metamaterials. *Science* **317** 1698–702

[5] Sihvola A 2007 Metamaterials in electromagnetics *Metamaterials.* **1** 2–11

[6] Lapine M, Powell D, Gorkunov M, Shadrivov I, Marqués R, Kisvshar Y 2009 Structural tunability in metamaterials *Appl. Phys. Lett.* **95** 084105.

[7] Shelby R A, Smith D R, and Schultz S 2001 Experimental verification of a negative index of refraction *Science* **292** 77-79.

[8] Giannini V, Fernández-Domínguez A I, Heck S C and Maier S A 2011 Plasmonic nanoantennas: Fundamentals and their use in controlling the radiative properties of nanoemitters *Chem. Rev.* **111** 3888–912

[9] Halas N J, Lal S, Chang W S, Link S and Nordlander P 2011 Plasmons in strongly coupled metallic nanostructures *Chem. Rev.* **111** 3913–61

[10] Evlyukhin A B, Novikov S M, Zywietz U, Eriksen R L, Reinhardt C, Bozhevolnyi S I and Chichkov B N 2012 Demonstration of magnetic dipole resonances of dielectric nanospheres in the visible region *Nano Lett.* **12** 3749–55

[11] García-Etxarri A, Gómez-Medina R, Froufe-Pérez L S, López C, Chantada L, Scheffold F, Aizpurua J, Nieto-Vesperinas M, Sáenz J J 2011 Strong magnetic response of submicron Silicon particle in the infrared *Opt. Express* **19** 4815-4826

[12] Gómez-Medina R, García-Cámara B, Súarez-Lacalle I, González F, Moreno F, Nieto-Vesperias M, Sáenz J J 2011 Electric and magnetic dipolar response of germanium nanospheres: interferecen effects, scattering anisotropy and optical forces *J. Nanophoton.* ***5*** *053512.*

[13] Evlyukhin A B, Reinhardt C, Seidel A, Luk'Yanchuk B S and Chichkov B N 2010 Optical response features of Si-nanoparticle arrays *Phys. Rev. B - Condens. Matter Mater. Phys.* **82** 1–12

[14] Lahiri B, McMeekin S G, Khokhar A Z, de la Rue R M and Johnson N P 2010 Magnetic response of split ring resonantors (SRRs) at visible frequencies *Opt. Express* **18** 3210-3218.

[15] Mirin N A, Halas N J 2009 Light-bending nanoparticles *Nano Lett.* **9**, 1255-1259.

[16] Kerker M, Wang D-S and Giles C L 1983 Electromagnetic scattering by magnetic spheres *J. Opt. Soc. Am.* **73** 765

[17] Rolly B, Stout B and Bonod N 2012 Boosting the directivity of optical antennas with magnetic and electric dipolar resonant particles *Opt. Express* **20** 20376

[18] Nieto-Vesperinas M, Gomez-Medina R and Saenz J J 2011 Angle-suppressed scattering and optical forces on submicrometer dielectric particles. *J. Opt. Soc. Am. A. Opt. Image Sci. Vis.* **28** 54–60

[19] Geffrin J M, García-Cámara B, Gómez-Medina R, Albella P, Froufe-Pérez L S, Eyraud C, Litman A, Vaillon R, González F, Nieto-Vesperinas M, Sáenz J J and Moreno F Magnetic and electric coherence in forward-and back-scattered electromagnetic waves by a single dielectric subwavelength sphere *Nat. Commun.* **3** 1171

[20] Fu Y H, Kuznetsov A I, Miroshnichenko A E, Yu Y F and Luk'yanchuk B 2013 Directional visible light scattering by silicon nanoparticles *Nat. Commun.* **4** 1527

[21] Liu W, Miroshnichenko A E, Neshev D N and Kivshar Y S 2012 Broadband unidirectional scattering by magneto-electric core-shell nanoparticles *ACS Nano* **6** 5489–97

[22] Krasnok A E, Miroshnichenko A E, Belov P A and Kivshar Y S 2012 All-dielectric optical nanoantennas *Opt. Express* **20** 20599–604

[23] Krasnok A E, Simovski C R, Belov P a and Kivshar Y S 2014 Superdirective dielectric nanoantennas. *Nanoscale* **6** 7354–61

[24] Filonov D S, Krasnok A E, Slobozhanyuk A P, Kapitanova P V., Nenasheva E A, Kivshar Y S and Belov P A 2012 Experimental verification of the concept of all-dielectric nanoantennas *Appl. Phys. Lett.* **100** 1–5

[25] Dietrich C P, Fiore A, Thompson M G, Kamp M, Höfling S 2016 GaAs integrate quantum photonics: Towards compact and multi-functional quantum photonic integrated circuits *Laser Photon. Rev.* **10**, 870-894.

[26] García-Cámara B, Gómez-Medina R, Sáenz J J, Sepúlveda B 2013 Sensing with magnetic dipolar resonances in semiconductor nanospheres *Opt. Express* **21** 23007-23020.

[27] Hillenbrand R, Keilmann F, Hanarp P, Sutherland D S and Aizpurua J 2003 Coherent imaging of nanoscale plasmon patterns with a carbon nanotube optical probe *Appl. Phys. Lett.* **83** 368–70
[28] Huber A J, Ocelic N and Hillenbrand R 2008 Local excitation and interference of surface phonon polaritons studied by near-field infrared microscopy *J. Microsc.* **229** 389–95
[29] Huber A J, Deutsch B, Novotny L and Hillenbrand R 2008 Focusing of surface phonon polaritons *Appl. Phys. Lett.* **92** 92–5
[30] Schnell M, Garcia-Etxarri A, Alkorta J, Aizpurua J and Hillenbrand R 2010 Phase-resolved mapping of the near-field vector and polarization state in nanoscale antenna gaps *Nano Lett.* **10** 3524–8
[31] García-Etxarri A, Romero I, García De Abajo F J, Hillenbrand R and Aizpurua J 2009 Influence of the tip in near-field imaging of nanoparticle plasmonic modes: Weak and strong coupling regimes *Phys. Rev. B - Condens. Matter Mater. Phys.* **79** 1–5
[32] Liu X, Qiu B, Chen Q, Ni Z, Jiang Y, Long M and Gui L 2014 Characterization of graphene layers using super resolution polarization parameter indirect microscopic imaging *Opt. Express* **22** 20446
[33] Ullah K, Liu X, Jichuan X, Hao J, Xu B, Jun Z and Liu W 2017 A Polarization Parametric Method of Sensing the Scattering Signals From a Submicrometer Particle *IEEE Photonics Technol. Lett.* **29** 19–22
[34] Bohren K F and Huffman D R 2004 *Absorption and Scattering of Light by Small Particles*
[35] García-Cámara B, Moreno F, González F, Saiz J M and Videen G 2008 Light scattering resonances in small particles with electric and magnetic properties. *J. Opt. Soc. Am. A. Opt. Image Sci. Vis.* **25** 327–34
[36] *www.sspectra.com/spectra.html.*
[37] Artar A, Yanik A A and Altug H 2011 Directional double Fano resonances in plasmonic hetero-oligomers *Nano Lett.* **11** 3694–700
[38] Fan J A, Bao K, Wu C, Bao J, Bardhan R, Halas N J, Manoharan V N, Shvets G, Nordlander P and Capasso F 2010 Fano-like interference in self-assembled plasmonic quadrumer clusters *Nano Lett.* **10** 4680–5
[39] Hao F, Nordlander P, Sonnefraud Y, Dorpe P Van and Maier S a 2009 Tunability of Subradiant Dipolar and Metallic Ring / Disk Cavities : Implications *Nano* **3** 643–52
[40] García-Cámara B G, Algorri J F, Cuadrado A, Urruchi V, Sánchez-pena J M and Vergaz R 2015 Size dependence of the Directional Scattering Conditions on Semiconductor Nanoparticles Size dependence of the Zero Backward and Minimum Forward Scattering Conditions on Semiconductor Nanoparticles **27** 2059–62
[41] Gómez-Medina R, García-Cámara B, Suárez-Lacalle I, González F, Moreno F, Nieto-Vesperinas M and Sáenz J J 2011 Electric and magnetic dipolar response of Germanium spheres: Interference effects, scattering anisotropy and optical forces *J. Nanophotonics* **5** 53512
[42] García-Etxarri A, Gómez-Medina R, Froufe-Pérez L S, López C, Chantada L, Scheffold F, Aizpurua J, Nieto-Vesperinas M and Sáenz J J 2011 Strong magnetic response of submicron silicon particles in the infrared. *Opt. Express* **19** 4815–26
[43] Zhang D F, Zhang H, Guo L, Zheng K, Han X D and Zhang Z 2009 Delicate control of crystallographic facet-oriented Cu2O nanocrystals and the correlated adsorption ability *J. Mater. Chem.* **19** 5220–5
[44] Powell D A, Lapine M,Gorkunov M, Shadrinov I V and Kivshar Y S 2010 Metamaterial tuning by manipulation of near-field interaction *Phys. Rev. B* **82** 155128.